Nanoscale

Accepted Manuscript

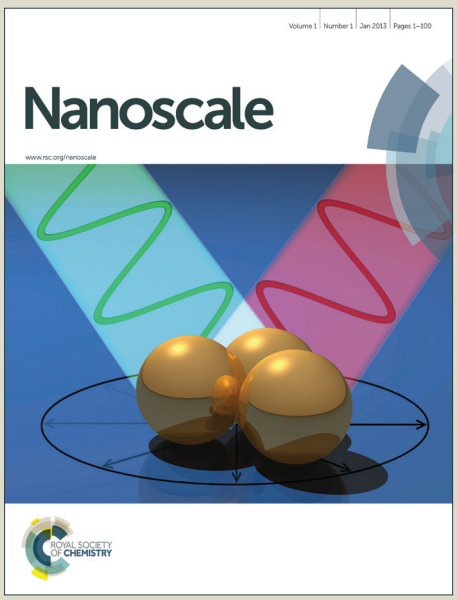

ROYAL SOCIETY OF CHEMISTRY

www.rsc.org/nanoscale

Photoelectron Spectroscopy of Wet and Gaseous Samples through Electron Transparent Graphene Membranes

Short title: Photoelectron Spectroscopy through Graphene Membranes

Authors:

Jürgen Kraus[1], *Robert Reichelt*[1], *Sebastian Günther*[1], *Luca Gregoratti*[2], *Matteo Amati*[2], *Maya Kiskinova*[2], *Alexander Yulaev*[3,5], *Ivan Vlassiouk* [4] *and Andrei Kolmakov*[5]*

[1]Technische Universität München D-85748 Garching, Germany

[2] Sincrotrone Trieste 34012 Trieste, Italy

[3]Department of Materials Science and Engineering, University of Maryland, College Park, MD 20742, USA

[4] Oak Ridge National Laboratory, Oak Ridge, TN 37831, USA

[5] Center for Nanoscale Science and Technology, NIST, Gaithersburg, MD 20899, USA

*Corresponfing author: Andrei Kolmakov

NIST 100 Bureau Drive

Bldg. 216/Rm.B117

Gaithersburg, MD 20899-6204

Phone: (301) 975-4724 Fax: (301) 975-2303

E-mail: andrei.kolmakov@nist.gov

Keywords: ambient pressure XPS, graphene membranes, spectromicroscopy

Abstract

Photoelectron spectroscopy (PES) and microscopy are highly demanded for exploring morphologically and chemically complex liquid-gas, solid-liquid and solid-gas interfaces under realistic conditions, but the very small electron mean free path inside the dense media imposes serious experimental challenges. Currently, near ambient pressure PES is conducted using dexterously designed electron energy analyzers coupled with differentially pumped electron lenses which made it possible conducting PES measurements at few hPa. This report proposes an alternative ambient pressure approach that can be applied to a broad class of samples and be implemented in conventional PES instruments. It uses ultrathin electron transparent but molecular impermeable membranes to isolate the high pressure sample environment from the high vacuum PES detection system. We demonstrate that the separating graphene membrane windows are both mechanically robust and sufficiently transparent for electrons in a wide energy range to allow soft X-ray PES of liquid and gaseous water. The performed proof-of-principle experiments confirm the possibility to probe vacuum-incompatible toxic or reactive samples placed inside such hermetic, gas flow or fluidic environmental cells.

1. Introduction

Ambient pressure *in situ* photoelectron spectroscopy (APPPES) with high energy and spatial resolution is very attractive for many important fields including catalysis[1, 2], fuel cells[3], batteries[4], environmental and atmospheric sciences[5] and bio-medical devices[6], where characterization of submicrometer structured matter and interfaces under operating conditions is prerequisite for further technological developments. Another fascinating application would be PES on surfaces of living microorganisms or biological cells. However, since the chemical information in PES is encoded in energies of the emitted photoelectrons, they have to be collected at a distance from the specimen comparable to the electron inelastic mean free path (IMFP), which for electron kinetic energies between 10^2 eV and 10^3 eV is about 1 nm for condensed matter and 1 μm for ambient pressure gases. This experimental challenge of bridging the so-called "pressure gap" has been judiciously addressed since the development of electron spectroscopy for chemical analysis (ESCA) in liquids by Kai Siegbahn's group in 1973[7]. The further development of their approach included liquid beams (jets [8-10], droplets on the fly[11]), wetted discs, wires and rods [12], pulsed gas delivery[13] but most of the efforts were focused on development of differentially pumped electron energy analyzers for solid samples in high pressure environment[14-16]. These achievements, reviewed in ref. [6, 17-19], have allowed routine PES measurements of reactive gases and liquids at pressures of a few hPa and a growing number of differentially pumped near-ambient pressure PES (APPES) instruments are operated in laboratories[20-22] and synchrotron facilities[23]. In the state-of-the art APPES stations (Figure 1 a) the achievable ultimate pressure around the sample is determined by interplay between a number of interrelated parameters such as electron IMFP in the specific gas, the distance D between the sample and the first differentially pumped aperture, the required electron count rate, the diameter

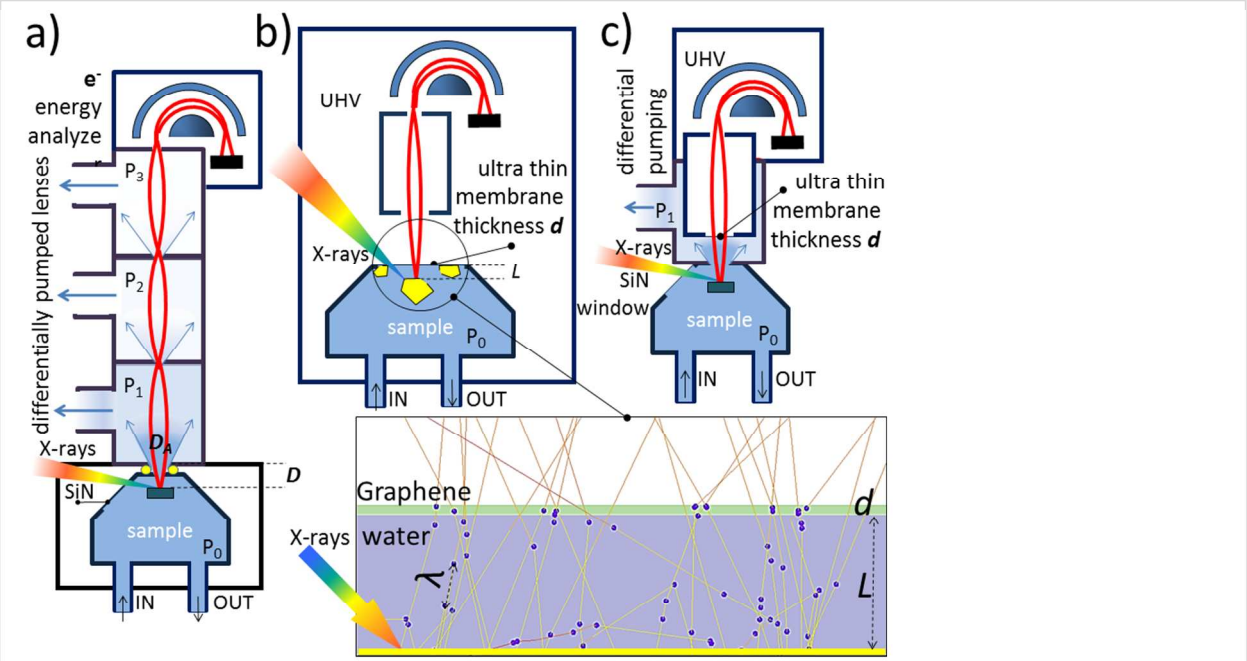

Figure 1. a) Currently employed APPES setup; b) Membrane based APPES used in the present study; inset: Monte Carlo simulation of 25 trajectories of 800 eV electrons emitted from the 20 nm sample covered with 5 nm water and single graphene layers. Dots represent individual scattering events. Note the existence of the trajectories with no electron scattering; c) an alternative scheme where the electron transparent membrane seals the lens of the electron energy analyzer.

of the aperture D_A, etc[24]. To avoid perturbation of the gas density near the sample by the reduced pressure at the front aperture, the distance D should be larger than D_A but also comparable with electrons IMFP (Figure. 1 a). The latter is in mm range for few hundred eV electrons propagating through 10^2 Pa of atmospheric gases. Since D_A has to be small enough to maintain required pressure differential but sufficiently large for transmission of a measurable electron flux, a practical compromise currently is using D_A of the order of a few hundred micrometers, which secures pressure of few hPa to be maintained around the sample. True atmospheric pressure has not been demonstrated yet but can in principle be envisioned with such a setup via further improvements in focusing of the X-rays to a submicron spot accompanied with D_A reduction and precise placement of the sample within few microns in front of the micron size first aperture. Here, we exploit another methodology for solving the 'pressure' problem using electron

transparent membranes. These are quasi-2D suspended films of thickness comparable to the electron IMFP and can be an alternative economic approach for separating the high pressure sample environment from the ultra-high vacuum (UHV) in the analyzer. The feasibility of this method stems from the successful PES analysis[25, 26] and imaging of buried interfaces using either UV[27] or hard X-rays excitation[28, 29]. The principle design of the membrane based PES approach is depicted in the Figure 1b. X-rays (or UV light) hit the sample which is located at distance *L* behind ultrathin membrane of thickness *d*. The photoelectrons travelling to the detector can be scattered both elastically and inelastically by the surrounding sample media and the membrane (see inset in the Figure 1b). The quantification of the photoelectron signal from the immersed sample is directly related to the classical surface science problem of signal attenuation by the overlayer films[26]. In the geometry illustrated in Figure 1b the attenuation due to inelastic electron scattering by dense medium of thickness *L* and membrane *d* can be evaluated as: $I/I_0 = \exp(-(\frac{L}{\lambda_M} + \frac{d}{\lambda_G}))$, where I_0 is initial intensity, λ_M and λ_G are IMFPs of the electrons in the dense media and membrane, respectively. The IMFPs for a few hundred eV electrons in condensed matter and gaseous environment at atmospheric pressure are of the order of 1 nm and 1 micrometer, respectively. Assuming 0.1 as an acceptable value for PES signal attenuation and membrane thickness of 1 nm, the probed sample surface can be located as far as 1 micrometer in ambient pressure environment (and about 100 micrometers at 10^3 Pa) from the membrane, i.e. far enough to maintain a facile molecular exchange and thermodynamic equilibrium with the ambient. Moreover, such setup would allow probing surfaces covered with several monolayers of liquid or solid media (inset in the Figure 1b). The minimal membrane thickness and sample-to-membrane distance requirements can be further relaxed if hard X-rays are used for PES, since photoelectrons in this case have high kinetic energies and therefore longer IMFPs[30]. Disposable

cells with electron transparent windows capable to achieve truly ambient conditions without sophisticated differential pumping and electron optics is advantageous feature of this approach.

Figure 1 c illustrates the third prospective approach that combines some features of the aforementioned schemes[31]. In this case the exchangeable electron transparent membrane assembly forms vacuum tight seal of the first lens of the standard electron energy analyzer. This will relax the requirement for multistage differential pumping since the membrane assembly design will allow withstanding the required pressure differential. The advantage of this approach is larger flexibility in samples exchange and their temperature variations. However, similar to the standard APPES setup the sample has to be in a close proximity to the membrane to maintain $D/\lambda_M \sim 1$ requirement.

In this communication we concentrate on the feasibility test of the ultrathin membranes as electron transparent windows separating UHV conditions in electron detector and ambient pressure environmental cells for APPES applications. Similar approach was first attempted in electron microscopy more than seventy years ago[32]. In spite of its long history (see recent review [33] and references therein), this approach has been hampered by the lack of membranes that are sufficiently electron transparent and yet mechanically robust enough to sustain needed10^5 Pa pressure differential. The recent progress in large-scale fabrication and handling protocols of novel two-dimensional materials such as graphene, graphene oxide, boron nitride, *etc.*, have ignited intensive studies of their exotic physical and chemical properties and multiple applications[34, 35]. The properties of these materials have revived the idea of photoelectron microscopy and spectroscopy through membranes that are reasonably transparent to photoelectrons with relatively low kinetic energy (less than 1 keV)[36-38]. These promising results, in conjunction with the reported mechanical stiffness and gas impermeability of graphene

membranes [39], have opened an alternative opportunity to probe a very broad class of materials and interfaces in their native environments using inexpensive disposable environmental cells. Reactive, toxic or radioactive materials in any state of aggregation can be tested using powerful electron spectroscopy and microscopy tools *i.e.* under experimental conditions which were not achievable before[38, 40].

Here we report proof-of-principle results demonstrating that, using suspended graphene as a separating membrane between vacuum and a liquid or dense gaseous medium, PES spectra of sufficient quality and low-electron-energy scanning electron microscopy (SEM) images of objects immersed in a liquid water environment can be recorded. Different from the prior demonstrations of XPS through graphene oxide (GO), graphene membranes offer principally new possibilities for APPES. Graphene being chemically and thermally stable, strongest and thinnest membrane possible meets excellently the demanding requirements of the electron transparent windows. Unlike GO, graphene is a conductor and, therefore, does not introduce potential energy reference problems due to charging of the membrane itself. What is most important: the high yield CMOS compatible fabrication and transfer protocols are readily available what brings the proposed methodology from academic research closer to the commercially feasible applications. The additional shortcomings of the GO drop casted membranes include: their susceptibility to thermal and chemical reduction by X-rays and electron beams; poor control over the final thickness of the membranes; the necessity of covering the micron size orifice with at least one individual GO flake to avoid the molecular permeability between overlapping flakes. There are two major approaches to fabricate suspended membranes made of high yield CVD grown graphene. One is based on local selective back etching of the native growth substrate (e.g. Cu, Ni) and the second one is realized via wet or dry transfer of the graphene from the growth substrate to secondary substrate with pre-patterned orifice(s)[41]. To test the applicability of both types suspended ultrathin single-use membrane

windows for *in situ* PES we compared achievable cleanness and electron transparency for photoelectrons with kinetic energies below 10^3 eV. Since it is difficult to measure IMFP of electrons directly, the experimentally accessible parameter electron attenuation length (EAL) is commonly used instead[42]. The EAL measurements were performed on graphene model samples. The feasibility of the performing near atmospheric pressure PES through the graphene windows has been demonstrated in this study by probing liquid water with μ-PES. Limiting factors such as water radiolysis at high irradiation doses are discussed.

2. Experiment

The experimental setup and procedures are described in the methods section and supporting

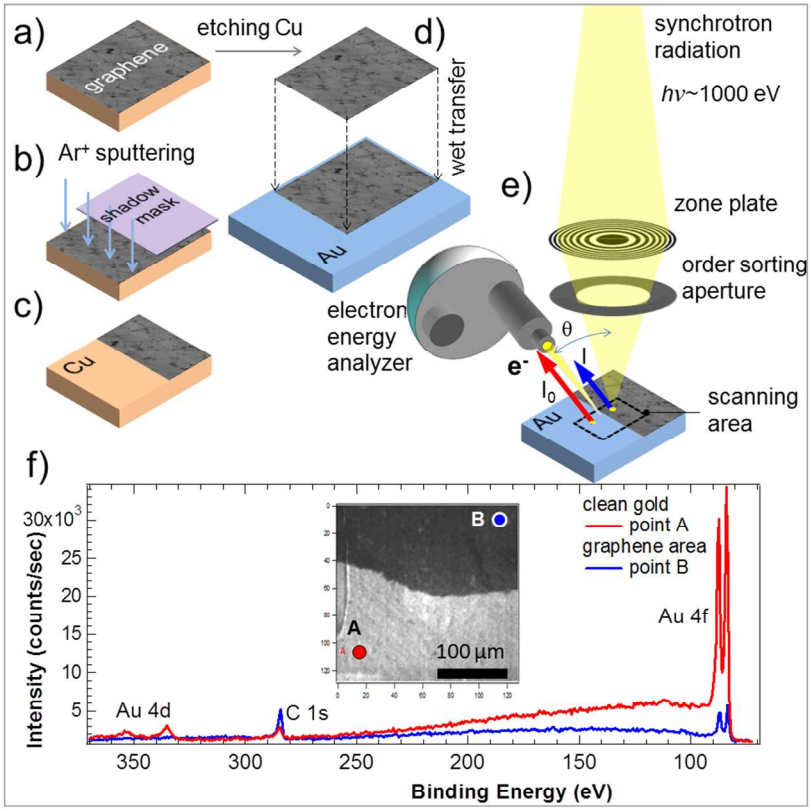

Figure 2. Sample preparation and experimental setup: a) as grown G layer on a Cu foil (g-Cu); b) Ar^+ sputtering of half of the sample using the shadow mask; c) Resultant pristine and graphene-covered Cu substrate for comparative XPS analysis; d) Alternative sample design using PMMA-based transfer of graphene on to a Au surface; e) Experimental setup of scanning photoelectron microscope at ELETTRA; f) (inset) 256 x 256 μm^2 Au 4f map of the half graphene-covered Au sample; Comparison of the XPS survey spectra acquired from points A and B in the inset. Significant attenuation of Au 4d, 4f peaks by the 4 ML thick graphene layer can be noticed

material. Briefly, monolayer graphene was grown by chemical vapor deposition (CVD) on 25 μm thick Cu foils (g-Cu) following a protocol described in Ref [43]. These samples were used for calibrating electron transparency and for preparation of suspended membranes via local chemical etching of the back side of Cu foil. For the fabrication of more robust graphene windows for liquid cells (so called environmental cells or E-cells) membranes with an average thickness of 4 ML were grown by CVD on Ni/Si substrates (Ni films deposited on Si wafers), chemically released and wet transferred[41] on to Au pre-covered support samples (g-Au) which contained orifices with diameter of a few micrometers. The design and tests of the E-cell as well as of the graphene-transfer protocols are described elsewhere[38]. It has been shown that to withstand ca 10^5 Pa pressure differential the suspended area of single layer graphene membranes should not exceed ca 10^2 μm^2.[39] Due to this small size, the PES experiments for probing the matter behind the suspended graphene-based membranes were performed using a focused X-ray beam (μ-probe PES or μ-PES)[44]. This setup allowed us to collect chemical maps at specific photoelectron energies as well as local PE spectra sequentially from the graphene-covered (g-Au) and adjacent bare areas of the Au substrate what is needed for electron transparency/attenuation measurements (Figure 2).

The similar comparative tests were performed with g-Cu samples where graphene was removed from part of the sample via sputtering through the shadow mask (Figure 2 a-c). In addition, to demonstrate the quality of the spectroscopy through graphene, we recorded spectra of the same suspended membranes before and after Au deposition on their back side. Finally, as a proof of principle, the real time physicochemical process such as evolution of the O1s photoelectron spectrum during water radiolysis was measured *in vivo* for the first time through the graphene membrane of vacuum-tight water filled E-cell.

3. Results and discussion

3.1 Attenuation tests for as grown and transferred g-samples

Figure 2f displays the measured signal attenuation of the Au 4f photoelectrons originating from the g-Au sample, half-covered by wet-transferred 4 ML thick graphene. Here, the Au 4f map identifies the edge of the transferred graphene film. The spectra acquired from the graphene-covered and the graphene-free areas reflect the considerable damping of the substrate signal by

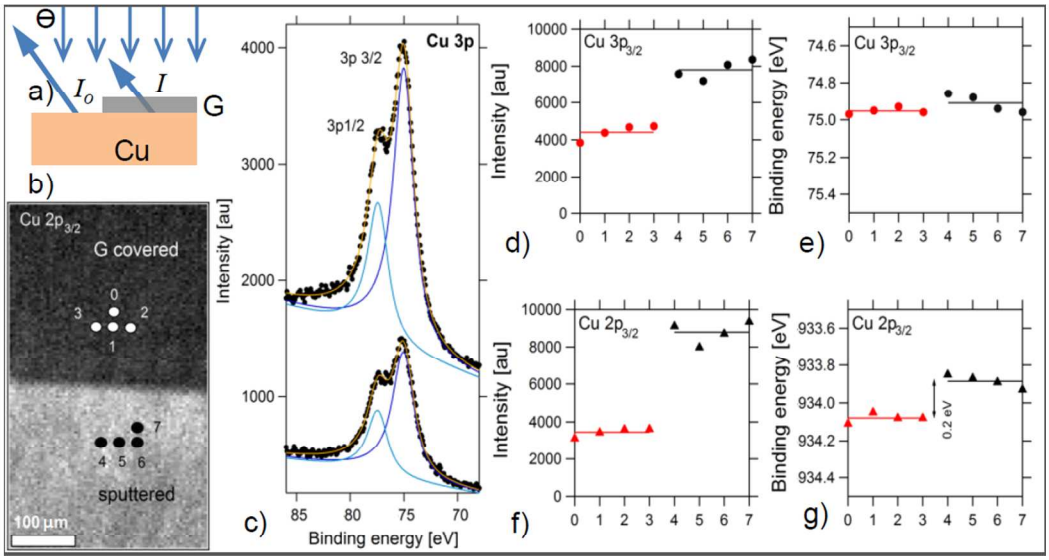

Figure 3 a) The geometry of the attenuation tests of g-Cu samples; b) Cu 2p map across the border of the g-covered and sputtered regions. The numbered points indicate the locations where the spectra are taken; c) typical Cu 3p spectra acquired from g-covered (bottom) and graphene-free (top) Cu regions where the deconvolution of the two components is shown as well; d) plot of the Cu $3p_{3/2}$ peak intensities measured from g-covered (points 0-3) and g-free (points 4-7) regions; e) Cu $3p_{3/2}$ peak position as a function of the location; f) and g) similar dependences as in d) and e) for Cu $2p_{3/2}$ spectra measured in the same locations, detecting photoelectrons with kinetic energy much lower than those for the Cu 3p spectra.

the wet-transferred graphene layer. We determined effective signal attenuation for the Au 4f photoelectrons of 85 % (at kinetic electron energy of 894 eV). Similar PES data were obtained from the partially sputter cleaned g-Cu sample, generating a border region between the graphene-covered and graphene-free Cu (see Figure 2a-c and 3 a, b). The acquired Cu 2p map across the border region is shown in Fig 3 b. The different intensity of the Cu 2p spectra in Figure 3c,

recorded at different locations on the graphene-free (black dots) and the graphene-covered parts of the Cu foil (white dots), is a result of the attenuation of the emitted Cu 3p photoelectrons by the graphene layer. The intensities for the deconvoluted Cu $2p_{3/2}$ and Cu $3p_{3/2}$ peaks at the different locations, indicated in Figure 3d and 3e, correspond to a signal attenuation by 66 % for Cu 2p (electron kinetic energy 138 eV) and 43 % for the Cu 3p (electron kinetic energy 997 eV). In addition, comparing the Cu 2p spectra recorded at graphene-free and graphene-covered areas we observed a small (≈ 0.2 eV) binding energy shift in the Cu $2p_{3/2}$ peaks positions (Figure 3g). Although the interfacial interactions between graphene and Cu transition metal are traditionally considered to be weak, this shift is in concert with the recently reported restructuring of the Cu surface underneath the CVD grown graphene[45, 46-48], which apparently is lifted after the graphene removal. As can be expected the interfacial graphene-Cu surface interactions are not affecting sensibly the energy positions of the Cu 3p spectra (Figure 3e), since the escape depth of the 1000 eV 3p Cu electrons is > 1.4 nm, so they are less sensitive to this surface phenomenon. We can now use measured I/I_0 intensity ratios for g-Au and g-Cu samples to determine electron attenuation lengths in these materials and compare them with values from the IMFP predictive formula for graphite by Tanuma, Powell and Penn (TPP-2M)[49] and also with the available Auger electron spectroscopy (AES) data[50] and our own laboratory XPS studies (see supplemental material and experimental section).

Further-on these EAL values are used to evaluate the thickness of the suspended and wet-transferred graphene membranes. Assuming a thickness of the graphene layer d_G = 3.35 Å, the electron effective attenuation length λ_{EAL} in monolayer graphene was estimated using the standard overlayer-film attenuation formula: $\lambda_{EAL} = d_G / \ln(I_0/I)\cos\theta$ (for the attenuation tests using conventional anodes, the electron emission angle θ = 0°). The experimental values for the

EAL are displayed in Figure 4A together with the IMFP for graphite, calculated applying the predictive TPP-2M equation (solid curve). In addition, the data from reference are added in the graph. One can see that the experimental data agree reasonably well with the values from the TTP-2M predictive formula using the set of parameters for graphite[50] and with the IMFP calculations based on optical data [49]. The systematic deviation of the EAL data to lower values, compared to the IMFPs, is presumably due to electron elastic scattering, which is taken into account in the λ_{EAL} values. It is notable that EALs for these low-Z single (or two) monolayer (ML) materials exceed or are comparable to their thicknesses for electron kinetic energy as low as 300 eV (dashed lines in the Fig 4A), which means that these materials are truly electron transparent even for these 'low' electron energy range.

We can now complement the electron attenuation data with electron transparency (I/I_0) data for

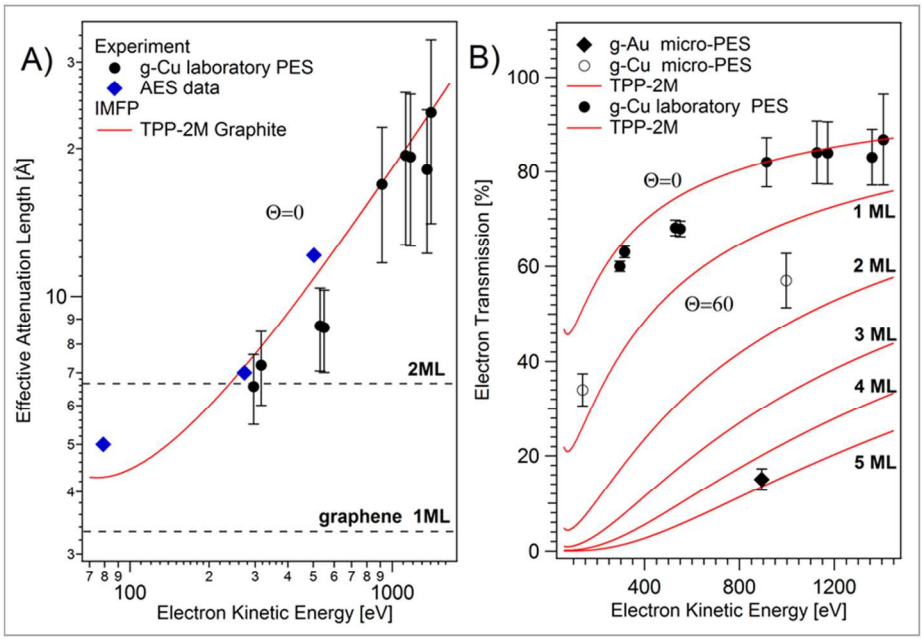

Figure 4. A) Solid line: inelastic mean free path in graphite as calculated using the optical data [49] and TPP-2M formula with the set of parameters from Ref. 50. Experimental data points (filled circles) represent the measured effective attenuation length (EAL) for graphene monolayer on Cu (g-Cu sample) for the Cu 2p, Cu 3s, Cu 3p and Cu LMM photoelectrons excited by Mg or Al Kα photons (emission angle θ = 0°). The EAL data (diamonds) from Ref. 50 are shown as well. The horizontal dashed lines indicate the thicknesses of single and bilayer graphene. B) Experimental data for electron transmission through single graphene layer, obtained using laboratory PES (filled circles) and a synchrotron-based μ-PES at with emission angle θ = 60° (open circles). The solid lines show the expected electron transparency (I/I_0) of graphene for different layer thickness, calculated using the TPP-2M IMFP formula. The filled diamonds correspond to wet transferred (g-Au sample) graphene with a nominal thickness of 4 ML, measured with the μ-PES.

the as-grown (g-Cu) and the transferred graphene layers (g-Au). The experimental μ-PES data points for graphene transparency in Figure 4B indicate that a significant photoelectron signal can be obtained from the samples placed behind a few ML thick graphene membranes. In fact, semi-empirical calculations indicate (see straight lines in the Figure 4B) that the electron transparency of a suspended single layer graphene membrane could be greater by 50 % for electron kinetic energies higher than 300 eV and only the elastic scattering will limit its transmissivity. Our data (filled and open symbols in the Fig 4B) support these predictions and justify the membrane concept both for environmental cells and for sealing the front lens of the electron analyzer. However, it can be expected that standard wet protocols for graphene transfer unavoidably introduces surface contaminations. Therefore, it is important to evaluate the degree of graphene contamination for this standard transfer protocol relating to the EAL expected from TTP-2M. To achieve this goal, the attenuation of electron intensity by a graphene layer with a nominal thickness of 4 ML was measured. Using λ_{EAL}=16.7 Å for Au 4f electrons with E_k=893 eV and the measured ratio of I/I_0=0.15 (see Figure 4b) one can evaluate the effective thickness of the transferred graphene as ≈ 5 ML, which corresponds to at least one monolayer of contaminants. Possible contamination sources are the remnant nanoscopic patches of the poly(methyl methacrylate) (PMMA) protection layer and solvents residue, which indeed can be observed, e.g. as Si 2p traces in the XPS data with an intensity corresponding to 0.4 ML.

We conducted the similar transparency tests on free suspended membranes made of g-Cu samples whose back-side was locally etched under controlled conditions producing graphene covered micro-holes (see details in the Methods section and the Supporting Material). The back side of these suspended membranes was covered with thin Au layer and Au 4f as well as C 1s intensities have been measures to determine the detection limit for soft X-ray PES through a

monolayer-thick graphene membrane. Assuming the validity of Volmer-Weber mode for Au growth on graphene[51, 52], the minimum gold amount detectable via Au 4f photoemission through a suspended monolayer graphene membrane was estimated to be lower than 1 % and 0.25 % of a monolayer respectively (see section 4 of supporting materials for details). This high sensitivity clearly demonstrates the potential of graphene-based membranes for studies of the matter behind the membrane.

3.2 Ambient pressure PES through g-membranes

To demonstrate the capability of ambient pressure PES through a graphene membrane, a 10 µL droplet of ultrapure water was placed on the membrane backside of an E-cell (Figure 5a) which was sealed in air to isolate the droplet from UHV of the µ-PES. Figures 5b and 5c show the chemical maps of the g-window and its surroundings acquired by collecting O 1s photoelectrons.

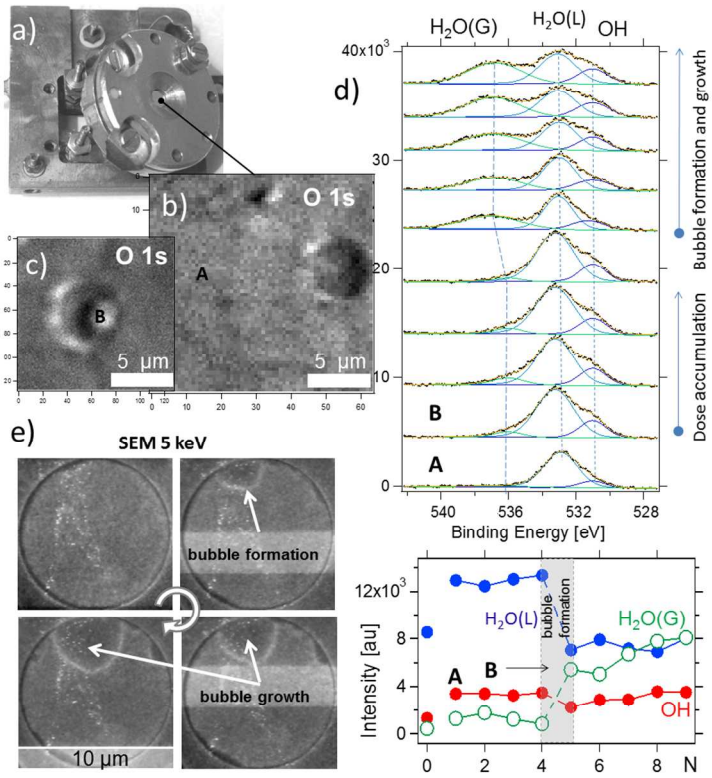

Figure 5. a) E-cell assembly; b) O1s maps of the graphene covered orifice before and after (c) spectra acquisition; d) successive O1s spectra taken from the location B showing the temporal evolution of liquid (L) and vapor (G) components of water band; for the sake of comparison the spectrum A recorded on the graphene covered support outside the membrane is displayed (point A in Figure5b); Bottom panel shows a plot of the intensity of the deconvoluted O 1s spectra as a function of time; e) SEM images of the beam-induced gas bubble nucleation and growth.

The contrast in each image is dominated by topographic features. Figure 5c depicts the area of Figure 5b after a prolonged exposure of point B inside the membrane window to the focused X-ray beam where the μ-PES data were taken. Figure 5d presents a set of sequentially measured O 1s spectra at point B starting from spectrum B. The bottom spectrum was taken in point A (Fig 5b), about 20 μm away from the membrane, while all other spectra were recorded in point B inside the membrane window (Figure 5c). The deconvolution of the O 1s spectrum was performed using three components, which are assigned to OH, H_2O (L) and H_2O (G), where *L* and *G* stand for liquid and vapor, respectively. These assignments are based on the relative positions and chemical shifts for surface hydroxyl groups, adsorbed molecular water and vapor measured with APPES of hydrated oxides[53] and micro jets[54]. In our experiments, the existence of molecular water and hydroxyl adsorbed species beyond the orifice can be attributed to a water monolayer that was trapped at the graphene-substrate interface during the wet transfer procedure and/or diffused from the orifice[55, 56]. Close inspection of the O 1s spectra clearly evidence that the first O 1s spectrum recorded from the membrane (point B) is significantly broadened and with higher intensity compared to the one from the graphene covered support (point A). These apparent differences are due to the fact that the liquid water below the membrane results in an increased photoelectron emission and the new components with water-related origin. The set of sequentially recorded O 1s spectra in the Figure 5 d (acquisition time of ≈ 30 s per spectrum) reveals noticeable changes in the O 1s peak lineshape as a function of the exposure time. This is due to variations in the weight of the different components, quantitatively depicted in the bottom panel of the Fig 5d. As can be seen, after exposure to the focused X-ray beam for about two minutes, a new O 1s component appears and grows at the expense of the liquid water H_2O (L) one. This new O 1s component corresponds to O 1s emission from water vapor H_2O (G), which

indicates X-ray beam-induced micro-bubble formation underneath the membrane, which also accounts for the bright spot in the O1s chemical map in the Figure 5c. Electron beam-induced micro-bubble formation and growth in liquids is regularly observed under high electron dosage [57] and was recently reported during scanning electron microscopy of the liquid water encapsulated by a graphene membrane[38]. In the latter case, the formation of the first bubble in water occurred after accumulation of a critical energy dose of ≈ 10^8 eV·nm^{-2} to 10^9 eV·nm^{-2} upon 20 keV electron beam irradiation. These values match the ones estimated from μ-PES experiment. This interpretation is further confirmed by four snapshots of a SEM video sequence recorded from water below a sealing graphene membrane (Figure 5e), where the time delay between the images is 10 s to 15 s. The reduced density of the liquid medium lowers the secondary electron yield so the darker round area in SEM images corresponds to a gas bubble formed at the interface between water and graphene. Under continuous electron beam raster, the bubble increases in size until occupying the entire area of the g-window (see the video in the Supporting Material). Following the enlightenments reported previously for liquid water[38, 57-59] and frozen hydrated samples [60], the bubble formation is primarily a result of water radiolysis by intense ionizing radiation. In our case, the X-ray energy dissipates in liquid water via creation of a variety of ionized and excited molecular and radical species in the interaction volume. Most of the ions and radicals recombine rapidly, but a few chemically reactive products, such as molecular hydrogen (H_2), hydrogen peroxide (H_2O_2) and hydroxyl radicals (·OH) accumulate [58] and eventually segregate as a separate phase towards the hydrophobic graphene membrane and form bubbles under the graphene membrane. This results in potential pressure buildup inside the E-cell and chemical etching of the membrane. Therefore, from the practical point of view the observed X-ray induced dynamic processes in liquid water are unwanted, since they obstruct interfacial

processes and limit the lifetime of the membrane. The natural solution of this experimental challenge will be the development a fluidic cell along with tuning of the lateral resolution, photon flux, electron collection dwell time, pass energy of the analyzer, etc. to the specific needs of the experiment.

4. Summary and prospective

We have developed and tested a novel APPES approach using graphene as an electron, X-ray, and optically transparent window, separating UHV analyzer chamber from the sample environment that allows for acquiring photoelectron spectra from fully hydrated interfaces. The evaluated transmissivity of single and multi-layer graphene for photoelectrons with kinetic energies in the range from ≈100 eV to 1 keV and different geometries of the PES setup demonstrate that our approach can complement current APPES technology, in particular in research areas where elevated pressures of liquid, gaseous, toxic, highly reactive, or even radioactive samples and interfaces are needed. These samples will be enclosed inside the hermetic microfluidic single use environmental cell and analyzed through the small electron-transparent window. The analysis of carbon containing samples will require a special attention sense XPS bands from such samples will have a dominating contribution from graphene membrane. Thorough peaks deconvolution procedures need to be implemented in spectral analysis in these cases. The class of suitable ultrathin window materials is not limited to graphene and its derivatives only. Recently high yield protocols for the fabrication of 2D and quasi-2D membranes made of BN, MoS_2, oxides, and other materials have been reported [61, 62]. This versatility in selection of electron-transparent window material will complement and broaden the possibilities of environmental electron spectroscopy and microscopy.

One of the limitations envisaged when attempting high spatial resolution studies in dense media are the X-ray or electron beam-induced effects. However, for a large class of experiments high spatial resolution is not required. To extend our technique to these applications we are developing special micro-porous substrates, which consist of high-density individually fillable micro-volumes as depicted in Figure 6. On the front side of such sample, nearly all micro-

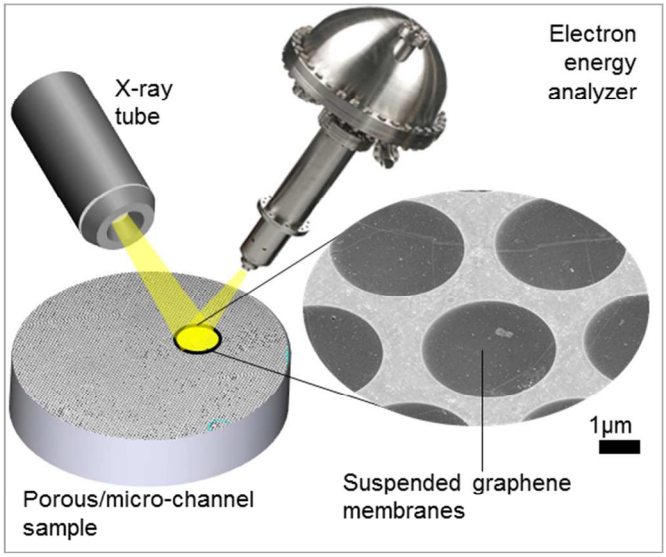

Figure 6. The principal concept of micro-porous substrates, which consist of the high-density individual micro-volumes separated from the vacuum by electron transparent membrane. The sample can be filled (impregnated) with the analyte which can be analyzed with standard laboratory XPS equipment.

volumes can be vacuum-sealed by the electron transparent membrane. An incidental disruption of a fraction of the individual micro-windows will not lead to complete sample loss since each micro-volume is isolated from the others. The surface coverage factor of this kind of sample can be as high as 50 %, making them suitable sample platform for analysis by standard PES equipment. In this case, the irradiation dose of liquid sample is reduced by more than two orders of magnitude compared to µ-PES setup thus eliminating water radiolysis related restrictions. This new set-up, which can also be used with other spectroscopic techniques sensitive to liquid (gas)-solid interfaces[63] is currently under final tests.

5. Experimental Section

5.1 Graphene samples. Monolayer graphene (g-Cu) was grown on 25 μm thick Cu foils in a CH_4/H_2 reactive atmosphere within the hPa pressure range following a protocol and at temperature of ≈1000°C, as described in Ref [43]. For the fabrication of more robust graphene windows for liquid cells, membranes with an average thickness of 4 monolayers were CVD grown on Ni films deposited on Si wafers. All samples were transported through air to the synchrotron facility ELETTRA, where further device preparation was performed prior to the μ-PES measurements.

We have tested two different approaches for fabrication of suspended membranes. In the first one the Cu foil underneath of the as-grown graphene was electrochemically etched. The etching was terminated as soon as the first few micrometer-sized optical holes appeared. Since on any graphene protective layer was used, such prepared suspended membranes have the highest electron transparency. The second type of membranes was produced via transferring of the graphene layer on to a Au-coated stainless steel support which contained a few micrometers' wide orifice using a modified PMMA transfer protocol (see details in [64]). To record the spectra from the wet sample through the graphene membrane, we used a custom-made single use E-cell (Figure 5a) described elsewhere[38]. The details of the graphene fabrication, SEM and Raman characterization, as well as the E-cell features, can be found in the supporting information.

5.2 Photoelectron spectroscopy and microscopy. Photoelectron attenuation tests were performed on as-grown graphene on Cu substrate foils (g-Cu) using a laboratory XPS system equipped with a non-monochromatic Mg Kα and Al Kα photon sources. The largest error affecting the precision of the attenuation tests is due to the need to switch-off the XPS apparatus

when removing the grown graphene layer by Ar^+ ion etching. The systematic error is of the order of ± 5 %, affects the extracted effective attenuation lengths which are indicated as error bars in Figure 4. The practical difference between these EAL and IMFP parameters is that EAL values take into account the elastic scattering inside the overlayer and thus depend on emission angle and the thickness of the overlayer. In our case the thickness of graphene is below 1 nm and the difference between these two parameters would not exceed the aforementioned error bar for electron emission angles used in this study. Therefore we can safely compare the measured and theoretical values of both of these parameters. The μ-PES measurements were performed using the scanning photoelectron microscope at the ELETTRA ESCA-microscopy beamline [65]. In the μ-PES setup, Fresnel zone plate optics was used to focus the X-ray beam onto a spot of *ca.* 100 nm in diameter (Figure 2e). The chemical, topography and transmission mapping of the sample can be obtained via raster scanning of the sample with respect to the focused X-ray beam with simultaneous collection of the element specific photoelectrons or transmitted photons. Detailed PES spectra can be acquired at any specific location selected from the maps. The incident angle of the X-ray beam and emission angle Θ of the electron analyzer were kept at 0° and 60°, respectively, with respect to the sample normal unless specified differently (see Figure 2e and Figure 3a). For quantitative analysis of the acquired data, the photoemission peaks were deconvoluted by Doniach-Sunjic line shapes[66].

5.3. Liquid sample preparation. Ultrapure 10 μL water droplet sample was pipetted on to the back side of the Au coated stainless steel disc with graphene covered micro-orifice. Inside E-cell assembly the sample was sealed with elastomer membrane. After the sealing, the E-cell was loaded at first in a load lock chamber, which was gradually evacuated, and then transferred to UHV μ-PES chamber. XPS imaging and spectroscopic measurements were performed *ca.* 1

hour after the cell was first exposed to vacuum. To minimize X-ray beam-induced damage of the g-membrane, care was taken to reduce the irradiation dose during the spectra acquisition by adjusting the X-ray focus accordingly. To avoid unnecessary exposure during the "parking" of the X-ray beam, the centered light spot was offset with respect to the center of the g-membrane resulting in a beam parking position outside the membrane.

Conflict of Interest: The authors declare no competing financial interest.

Supporting Information

Supporting Information is available on line.

Acknowledgements:

The suggestions and comments from Drs. N. Zhitenev, Ch. Brown, D. Meier, R. Sharma and C. Powell (all at NIST) are greatly acknowledged. This work made extensive use NIST SRD-82 EAL and NIST -71 IMFP databases, for which the authors are thankful to Drs. C. J. Powell and A. Jablonski. S.G. gratefully acknowledges financial support from the German Science Foundation (DFG, contract number GU 521/2-1)

References

1. A. Knop-Gericke, E. Kleimenov, M. Hävecker, R. Blume, D. Teschner, S. Zafeiratos, R. Schlögl, V. I. Bukhtiyarov, V. V. Kaichev and I. P. Prosvirin, *Advances in Catalysis*, 2009, 52, 213-272.
2. G. A. Somorjai, R. L. York, D. Butcher and J. Y. Park, *Physical Chemistry Chemical Physics*, 2007, 9, 3500-3513.
3. C. Zhang, M. E. Grass, A. H. McDaniel, S. C. DeCaluwe, F. El Gabaly, Z. Liu, K. F. McCarty, R. L. Farrow, M. A. Linne and Z. Hussain, *Nature materials*, 2010, 9, 944-949.
4. Y.-C. Lu, E. J. Crumlin, G. M. Veith, J. R. Harding, E. Mutoro, L. Baggetto, N. J. Dudney, Z. Liu and Y. Shao-Horn, *Scientific reports*, 2012, 2.
5. S. Ghosal, J. C. Hemminger, H. Bluhm, B. S. Mun, E. L. Hebenstreit, G. Ketteler, D. F. Ogletree, F. G. Requejo and M. Salmeron, *Science*, 2005, 307, 563-566.
6. G. Ketteler, P. Ashby, B. S. Mun, I. Ratera, H. Bluhm, B. Kasemo and M. Salmeron, *J Phys-Condens Mat*, 2008, 20.
7. H. Siegbahn and K. Siegbahn, *Journal of Electron Spectroscopy and Related Phenomena*, 1973, 2, 319-325.

8. H. Siegbarn, L. Asplund, P. Kelfve, K. Hamrin, L. Karlsson and K. Siegbahn, *Journal of Electron Spectroscopy and Related Phenomena*, 1974, 5, 1059-1079.
9. B. Winter and M. Faubel, *Chemical reviews*, 2006, 106, 1176-1211.
10. M. A. Brown, I. Jordan, A. B. Redondo, A. Kleibert, H. J. Wörner and J. A. van Bokhoven, *Surface Science*, 2013.
11. D. E. Starr, E. K. Wong, D. R. Worsnop, K. R. Wilson and H. Bluhm, *Physical Chemistry Chemical Physics*, 2008, 10, 3093-3098.
12. H. Siegbahn, *The Journal of Physical Chemistry*, 1985, 89, 897-909.
13. M. Amati, M. K. Abyaneh and L. Gregoratti, *Journal of Instrumentation*, 2013, 8, T05001.
14. R. W. Joyner, M. W. Roberts and K. Yates, *Surface Science*, 1979, 87, 501-509.
15. H. Ruppender, M. Grunze, C. Kong and M. Wilmers, *Surface and interface analysis*, 1990, 15, 245-253.
16. D. F. Ogletree, H. Bluhm, G. Lebedev, C. S. Fadley, Z. Hussain and M. Salmeron, *Review of Scientific Instruments*, 2002, 73, 3872-3877.
17. M. Salmeron and R. Schlogl, *Surf Sci Rep*, 2008, 63, 169-199.
18. D. Starr, Z. Liu, M. Hävecker, A. Knop-Gericke and H. Bluhm, *Chemical Society Reviews*, 2013.
19. B. S. Mun, H. Kondoh, Z. Liu, P. N. Ross Jr and Z. Hussain, in *Current Trends of Surface Science and Catalysis*, Springer, 2014, pp. 197-229.
20. F. Tao, *Chemcatchem*, 2012, 4, 583-590.
21. A. Jurgensen, N. Esser and R. Hergenroder, *Surface and Interface Analysis*, 2012, 44, 1100-1103.
22. K. Roy, C. Vinod and C. S. Gopinath, *The Journal of Physical Chemistry C*, 2013, 117, 4717-4726.
23. J. Schnadt, J. Knudsen, J. N. Andersen, H. Siegbahn, A. Pietzsch, F. Hennies, N. Johansson, N. Martensson, G. Ohrwall and S. Bahr, *Journal of synchrotron radiation*, 2012, 19, 701-704.
24. D. Frank Ogletree, H. Bluhm, E. D. Hebenstreit and M. Salmeron, *Nuclear Instruments and Methods in Physics Research Section A: Accelerators, Spectrometers, Detectors and Associated Equipment*, 2009, 601, 151-160.
25. A. Jablonski and C. J. Powell, *Journal of Vacuum Science & Technology A*, 2009, 27, 253-261.
26. D. Briggs and M. P. Seah, *Practical Surface Analysis by Auger and X-ray Photoelectron Spectroscopy*, John Wiley & Sons Ltd 1983.
27. V. Ballarotto, M. Breban, K. Siegrist, R. Phaneuf and E. Williams, *Journal of Vacuum Science & Technology B*, 2002, 20, 2514-2518.
28. T. Wakita, T. Taniuchi, K. Ono, M. Suzuki, N. Kawamura, M. Takagaki, H. Miyagawa, F. Guo, T. Nakamura and T. Muro, *Japanese journal of applied physics*, 2006, 45, 1886.
29. K. Kobayashi, *Nuclear Instruments and Methods in Physics Research Section A: Accelerators, Spectrometers, Detectors and Associated Equipment*, 2009, 601, 32-47.
30. T. Masuda, H. Yoshikawa, H. Noguchi, T. Kawasaki, M. Kobata, K. Kobayashi and K. Uosaki, *Applied Physics Letters*, 2013, 103, 111605-111605-111604.
31. 2004.
32. I. M. Abrams and J. W. McBain, *Journal of Applied Physics*, 1944, 15, 607-609.
33. N. de Jonge and F. M. Ross, *Nat Nano*, 2011, 6, 695-704.
34. K. Novoselov, D. Jiang, F. Schedin, T. Booth, V. Khotkevich, S. Morozov and A. Geim, *Proceedings of the National Academy of Sciences of the United States of America*, 2005, 102, 10451-10453.
35. S. Park and R. S. Ruoff, *Nature nanotechnology*, 2009, 4, 217-224.
36. J. Mutus, L. Livadaru, J. Robinson, R. Urban, M. Salomons, M. Cloutier and R. Wolkow, *New Journal of Physics*, 2011, 13, 063011.
37. A. Kolmakov, D. A. Dikin, L. J. Cote, J. Huang, M. K. Abyaneh, M. Amati, L. Gregoratti, S. Günther and M. Kiskinova, *Nature Nanotechnology*, 2011, 6, 651-657.
38. J. D. Stoll and A. Kolmakov, *Nanotechnology*, 2012, 23, 505704.

39. J. S. Bunch, S. S. Verbridge, J. S. Alden, A. M. van der Zande, J. M. Parpia, H. G. Craighead and P. L. McEuen, *Nano letters*, 2008, 8, 2458-2462.
40. J. M. Yuk, J. Park, P. Ercius, K. Kim, D. J. Hellebusch, M. F. Crommie, J. Y. Lee, A. Zettl and A. P. Alivisatos, *Science*, 2012, 336, 61-64.
41. J. W. Suk, A. Kitt, C. W. Magnuson, Y. Hao, S. Ahmed, J. An, A. K. Swan, B. B. Goldberg and R. S. Ruoff, *ACS nano*, 2011, 5, 6916-6924.
42. C. Powell and A. Jablonski, *Surface and interface analysis*, 2002, 33, 211-229.
43. X. Li, W. Cai, J. An, S. Kim, J. Nah, D. Yang, R. Piner, A. Velamakanni, I. Jung, E. Tutuc, S. K. Banerjee, L. Colombo and R. S. Ruoff, *Science*, 2009, 324, 1312-1314.
44. A. Barinov, P. Dudin, L. Gregoratti, A. Locatelli, T. O. Mentes, M. A. Nino and M. Kiskinova, *Nucl Instrum Meth A*, 2009, 601, 195-202.
45. H. I. Rasool, E. B. Song, M. Mecklenburg, B. Regan, K. L. Wang, B. H. Weiller and J. K. Gimzewski, *Journal of the American Chemical Society*, 2011, 133, 12536-12543.
46. J. Cho, L. Gao, J. Tian, H. Cao, W. Wu, Q. Yu, E. N. Yitamben, B. Fisher, J. R. Guest and Y. P. Chen, *ACS nano*, 2011, 5, 3607-3613.
47. L. Gao, J. R. Guest and N. P. Guisinger, *Nano letters*, 2010, 10, 3512-3516.
48. J. Kraus, S. Böcklein, R. Reichelt, S. Günther, B. Santos, T. O. Menteş and A. Locatelli, *Carbon*, 2013, 64, 377-390.
49. S. Tanuma, C. Powell and D. Penn, *Surface and Interface Analysis*, 2011, 43, 689-713.
50. M. Xu, D. Fujita, J. Gao and N. Hanagata, *Acs Nano*, 2010, 4, 2937-2945.
51. H. Hövel and I. Barke, *Progress in surface science*, 2006, 81, 53-111.
52. M. Büttner and P. Oelhafen, *Surface science*, 2006, 600, 1170-1177.
53. G. Ketteler, S. Yamamoto, H. Bluhm, K. Andersson, D. E. Starr, D. F. Ogletree, H. Ogasawara, A. Nilsson and M. Salmeron, *The Journal of Physical Chemistry C*, 2007, 111, 8278-8282.
54. K. M. Lange, A. Kothe and E. F. Aziz, *Physical Chemistry Chemical Physics*, 2012, 14, 5331-5338.
55. E. Stolyarova, D. Stolyarov, K. Bolotin, S. Ryu, L. Liu, K. Rim, M. Klima, M. Hybertsen, I. Pogorelsky and I. Pavlishin, *Nano letters*, 2008, 9, 332-337.
56. K. Xu, P. Cao and J. R. Heath, *Science*, 2010, 329, 1188-1191.
57. J. M. Grogan, N. M. Schneider, F. M. Ross and H. H. Bau, *Nano Letters*, 2013, DOI: 10.1021/nl404169a.
58. C. Royall, B. Thiel and A. Donald, *Journal of Microscopy*, 2001, 204, 185-195.
59. S. Thiberge, O. Zik and E. Moses, *Review of Scientific Instruments*, 2004, 75, 2280-2289.
60. R. D. Leapman and S. Sun, *Ultramicroscopy*, 1995, 59, 71-79.
61. L. Wang, J. J. Travis, A. S. Cavanagh, X. Liu, S. P. Koenig, P. Y. Huang, S. M. George and J. S. Bunch, *Nano letters*, 2012, 12, 3706-3710.
62. A. Neto and K. Novoselov, *Materials Express*, 2011, 1, 10-17.
63. F. Zaera, *Chemical Reviews*, 2012, 112, 2920-2986.
64. X. Li, Y. Zhu, W. Cai, M. Borysiak, B. Han, D. Chen, R. D. Piner, L. Colombo and R. S. Ruoff, *Nano letters*, 2009, 9, 4359-4363.
65. M. K. Abyaneh, L. Gregoratti, M. Amati, M. Dalmiglio and M. Kiskinova, *e-Journal of Surface Science and Nanotechnology*, 2011, 9, 158-162.
66. J. More, *Numerical analysis*, 1978, 105-116.

Table of contents entry

Photoelectron spectroscopy proves to be among the most surface-sensitive and informative techniques. However, it is hard to apply to objects immersed into realistic environments such as liquid or atmospheric pressure gases due to very short electron mean free path in these dense media. In this paper, we overcome this limitation by employing ultra-thin electron transparent membranes such as graphene to separate the sample environment from the high vacuum conditions in the electron spectrometer.

Keywords: ambient pressure XPS, graphene membranes, spectromicroscopy

Authors: Jürgen Kraus, Robert Reichelt, Sebastian Günther, Luca Gregoratti, Matteo Amati, Maya Kiskinova, Alexander Yulaev, Ivan Vlassiouk and Andrei Kolmakov*

Photoelectron Spectroscopy of Wet and Gaseous Samples through Electron Transparent Graphene Membranes

ToC Figure